Real-Time Testing of a Fuzzy-Logic-Controller-Based Grid-Connected Photovoltaic Inverter System

M. A. Hannan, Zamre Abd. Ghani, Azah Mohamed, *Senior Member, IEEE*, and M. Nasir Uddin, *Senior Member, IEEE*

***Abstract*—This paper presents a novel fuzzy-logic-based high-performance control of a three-phase photovoltaic grid-connected inverter. With the aid of the inverter model and fuzzy-logic-based voltage and current-control schemes, a digital signal processor controller board DS1104 generates the sinusoidal pulsewidth modulated signals for the inverter operation in both stand-alone and grid-connected modes. An inverter prototype was built to verify the effectiveness of the control algorithm. The system demonstrates stable ac output voltage satisfactorily during both transient and steady state with grid and load disturbances. The control system generates 2.48% and 4.64% voltage and current total harmonic distortions, respectively. The output waveforms such as output voltage, injected current, and the system power flow are presented to validate the effectiveness of the control strategy.**

***Index Terms*—Current control, fuzzy logic controller (FLC), grid-connected photovoltaic (PV) system, real-time testing, three-phase inverter, voltage control.**

NOMENCLATURE

R_s	Internal resistance of stack.
I_c	Output current of the solar cell.
$I_{\rm ph}$	Light-generated cell current.
I_o	Diode reverse saturation current.
$I_{\rm sat}$	Diode saturated current.
T_c	Cell temperature in Kelvin.
A	Ideality factor.
K	Boltzmann constant.
q	Electron charge.
G	Irradiance.
β	Voltage temperature coefficient.
N_s	Modules number in series.
N_p	Modules number in parallel.
α	Current temperature coefficient.
$I_{\rm pv}$	Output current of the PV array.
$P_{\rm pv}$	Output power of the PV array.
T	Stack temperature.
$V_{\rm ref}$	PV reference voltage.
$I_{\rm ref}$	PV reference current.
$T_{\rm ref}$	Reference stack temperature.

Manuscript received October 20, 2014; revised May 8, 2015; accepted July 3, 2015. Date of publication July 10, 2015; date of current version November 18, 2015. Paper 2014-IACC-0723.R1, presented at the 2014 IEEE Industry Applications Society Annual Meeting, Vancouver, BC, Canada, October 5–9, and approved for publication in the IEEE TRANSACTIONS ON INDUSTRY APPLICATIONS by the Industrial Automation and Control Committee of the IEEE Industry Applications Society. This work was supported by the Ministry of Science, Technology and Innovation, Malaysia, under Grant DPP-2014-143 and Grant 06-01-02-SF1060.

M. A. Hannan and A. Mohamed are with the Department of Electrical, Electronic and Systems Engineering, Universiti Kebangsaan Malaysia, 43600 Bangi Selangor, Malaysia (e-mail: hannan@eng.ukm.my; azah@eng.ukm.my).

Z. A. Ghani is with the Department of Electronic and Computer Engineering, Universiti Teknikal Malaysia, 76100 Melaka, Malaysia (e-mail: zamre@utem.edu.my).

M. N. Uddin is with the Department of Electrical Engineering, Lakehead University, Thunder Bay, ON P7B 5E1, Canada (e-mail: muddin@lakeheadu.ca).

Color versions of one or more of the figures in this paper are available online at http://ieeexplore.ieee.org.

Digital Object Identifier 10.1109/TIA.2015.2455025

I. INTRODUCTION

The photovoltaic (PV) system has been becoming one of the important renewable energy sources due to its availability and easy access. Since it is a dc power source, an inverter is necessary to convert it to ac power, which can be used to power up ac loads or can be transported to the utility grid [1]. In addition, with proper energy management, the PV power system has become valuable and significant particularly for remote area users, where the utility is unavailable [2]. The success of the PV power utilization is associated with proper control techniques of the inverter [3]. Researchers have been focusing on various inverter control issues, including self-consumption losses [4], nonlinearity behavior, output fluctuation, weather dependence and low efficiency of PV [5], electromagnetic interference, harmonics distortion level [6], dc bus voltage fluctuations [7], and attainment of unity power factor [8]. Thus, the design of the inverter controller is a crucial issue for the overall PV system performance [9]–[13]. For easier implementation, researchers utilized various types of proportional–integral (PI), and PI-derivative (PID) controllers to control the PV inverter [14]. There have been considerable research works done in the area of single-phase grid-connected PV inverter using PI, proportional resonant integral (PRI), quasi-proportional resonance (QPR) control methods to reduce harmonic distortion, speed up the system response, and maintain the frequency stability [15]–[18]. However, the well-known disadvantages on larger output filter, discretization of grid frequency, and lack of intelligence level of the conventional PI, PID, PRI, QPR controllers, and their adaptive versions encourage researchers to apply the intelligent controllers such fuzzy logic, neural network, neurofuzzy, genetic algorithm, etc., for PV inverter system [19]–[23]. An adaptive-neurofuzzy-inference-system (ANFIS)-based supervisory control for three-phase grid-connected inverter system is developed in order to

TABLE I
SUMMARY OF INVERTERS PARAMETERS IN RELATION TO REFERENCES

Inverter Parameters	Ref. 6	Ref. 9	Ref. 10	Ref. 11	Ref. 12	Ref.13	Ref. 27
Voltage THD	N/A	N/A	N/A	N/A	6.8%	N/A	1.5%
Current THD	6.8	4.0	8.4	8.87	N/A	19.8	N/A
Power Factor	N/A	N/A	0.96	0.994	unity	unity	N/A
Topology	3-Ø 3-L	3-Ø 3-L	1-Ø 5-L	3-Ø 3-L	1-Ø 5-L	3-Ø 3-L	3-Ø 3-L
Switching Technology	PWM	SVPWM	SPWM	SPWM	SPWM	SPWM	PWM
Hardware	Simple	mod	mod	mod	complex	complex	complex
System	Progm	Progm / Simulink	Progm	Progm	Progm	Progm	Progm
Transformer	Yes	no	no	no	no	no	no

* N/A- not available, L-level, mod -moderate, Progm -programming

maintain availability of the grid power demand. However, in the case of large data sets, the ANFIS network training is a problem [24]. The main advantages of intelligent controllers are their designs do not need the exact mathematical model of the system, and theoretically, they are capable of handling any nonlinearity of arbitrary complexity. Thus, the intelligent controllers are perfect candidates for controlling PV inverter system as the Sun, which is the main source for PV system is unpredictable.

Among the various intelligent controllers, fuzzy logic controller (FLC) is the simplest for inverter control. The FLC is better than the conventional controllers in terms of insensitivity to parameter and load variations, response time, settling time, and robustness [25]. Table I presents the summary of inverters system parameters in terms of the output voltage and current harmonics contents, power factor, topology, switching method, implementation, system environment or platform, and utilization of transformers.

Apparently, the design of inverters without the transformers seems to be more favorable as it improves the overall inverter physical size and weight [26]. The level of difficulties on the system implementation is associated with the inverter topology, switching topology, and system environment or platform. In regard to the topology and control algorithm, two- or three-level types of inverters are simple to be implemented. Multilevel inverters, i.e., above five levels, require a complex control algorithm particularly, in switching signals generation and system coordination, which adds computational burden to the processor [27]. Moreover, the increased number of semiconductor switches causes the overall system costly [28].

Therefore, in this paper a new fuzzy logic control strategy is developed for high-performance control of grid-connected three-phase PV inverter system. In order to a test the effectiveness of the proposed control technique, a 3-kW prototype PV grid-connected three-phase inverter is built using the DSP board DS 1104. The proposed FLC demonstrates stable ac output voltage of the inverter satisfactorily during both transient and steady-state conditions, including the grid and/or load disturbances. Moreover, the inverter is capable of feeding excess power to the grid when the power generation is more than local demand. The developed control system generates only 2.48% and 4.64% of output voltage and current total harmonic distortions (THDs), respectively. The output waveform results such as the inverter output voltage, injected current, and the system power flow are presented to validate the effectiveness of the control system. The developed FLC control system also exhibits better performance in reducing the output voltage and current overshoots, as compared with that of the PI controller.

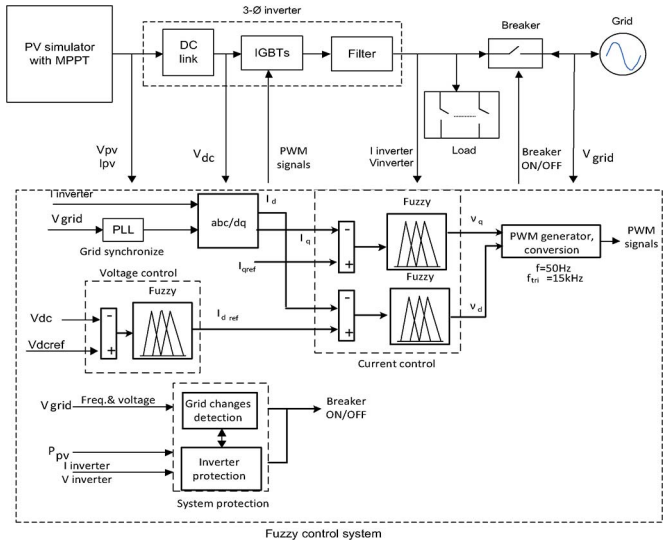

Fig. 1. Overall control scheme for PV-based inverter system.

II. PV-BASED GRID-CONNECTED INVERTER SYSTEM

The configuration of the PV-based three-phase grid-connected voltage-source inverter system considered in this paper is illustrated in Fig. 1.

It consists of an FLC control system, PV simulator, inverter, and load. The control system consists of several subcontrol modules, which include voltage and current-control functions, grid synchronization, pulsewidth modulated (PWM) signal generator, abnormal voltage detections such as over- and under-voltage and frequency. By means of the output parameters sampling such as voltage and current, and implementation of control and maximum power point tracking (MPPT) algorithm, the system controller managed to transfer the maximum PV power to the load, as well as stabilizes the ac output voltage, current, and frequency to the desired levels. These objectives are accomplished with the generation of PWM signals for the inverter switching devices. A controllable breaker is used for connecting and disconnecting the inverter to the grid line.

The PV simulators with a built-in dc–dc boost converter along with perturb-and-observe (P&O)-based MPPT algorithm generates the suitable and regulated dc power required by the inverter. In P&O, the PV parameters, e.g., voltage or current is increased or decreased continuously in order to extract the maximum power from the PV panel. The block diagram of the PV simulator is shown in Fig. 2(a). Detailed MPPT method and algorithm can be found in [29]. With the MPPT feature, the PV system transfers maximum power at different solar irradiations. The PV output parameters vary at different solar irradiations and temperature. In this paper, for simplification, the implementation is executed only at a fixed solar irradiation

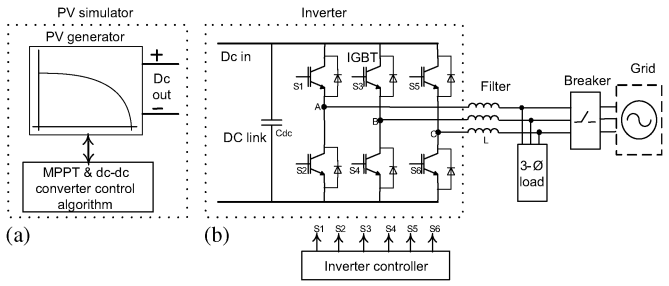

Fig. 2. Three-phase grid-connected (a) PV simulator and (b) inverter topology.

of 1000 W/m^2 at 25 °C. The parameters of the PV module includes the open circuit voltage, $V_{\rm oc}$ (21.8 V), short-circuit current, $I_{\rm sc}$ (5 A), voltage at maximum power, $V_{\rm mp}$ (17 V), and current at maximum power, $I_{\rm mp}$ (4.7 A). The PV array is formed by modules connected in series-parallel combinations to produce total dc output voltage of 408 V with a power capacity of 5.8 kW to be fed to the dc–dc boost converter. In principle, the output voltage of the solar cell is a function of the photocurrent that depends on the solar irradiation level during its operation. The output current of the solar cell can be represented as

$$I_c = I_{\rm ph} - I_o = I_{\rm ph} - I_{\rm sat}\left[e^{\frac{q}{AKT_c}(V+IR_S)} - 1\right]. \quad (1)$$

The voltage and current generated by the PV system depend on the combination of N_s (number of series module) and N_p (number of parallel branch) of PV arrays, which are given by (2) and (3), respectively,

$$V_{\rm PV} = N_S\left(V_{\rm ref} - \beta(T - T_{\rm ref}) - R_s \quad (2)$$

$$I_{\rm PV} = N_P\left(I_{\rm ref} + \alpha\left(\frac{G}{1000}\right)(T - T_{\rm ref}) + \left(\frac{G}{1000} - 1\right)I_{\rm sc}\right). \quad (3)$$

The power output of the PV array is given by [25]

$$P_{\rm PV} = I_{\rm PV} \times V_{\rm PV}. \quad (4)$$

By utilizing the dc–dc boost converter, the PV voltage, $V_{\rm pv}$ is stepped-up to 700 V for the inverter dc input voltage, $V_{\rm dc}$. This is achieved by varying the duty cycle, D of the power device using the PWM method, as described in

$$V_{\rm dc} = \frac{V_{\rm PV}}{1 - D}. \quad (5)$$

The topology of the three-phase inverter is shown in Fig. 2(b). It consists of mainly a dc link, power stage [insulated-gate bipolar transistor (IGBT) inverter], and filters. The dc link consists of a 30 μF capacitor, which links the dc power to the inverter system. Its high capacitance helps to stabilize the input voltage for the inverter. The inverter is connected to the grid through filter inductor of 1.8 mH in each phase which reduces the high-frequency harmonic components injected to the grid system [31]. The PWM logic signals S1, S2, S3, S4, S5, and S6 for the inverter switches are generated by the controller based on the inverter output parameters and strategy of control algorithm.

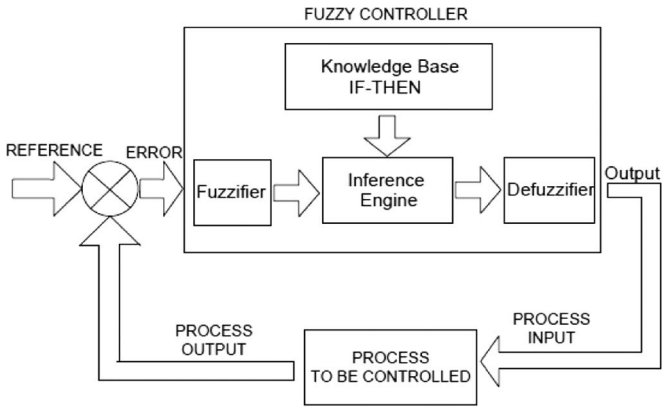

Fig. 3. Fuzzy logic control architecture.

A. Overall Control Principle

The control strategy for the switching signals generation consists of several functional components such as phase-locked loop-type grid synchronization, $abc-dq0$ coordinate transformation, voltage and current regulations, fuzzy-logic controllers, system protections, PWM signals generation and signals conversion.

Initially, in a stand-alone or off-grid mode, the inverter operates undervoltage-controlled scheme and supplies power to the ac loads. The inverter ac output voltage is sensed and converted to $dq0$ components by utilizing the Park's transformation. This is done to ease the three-phase analysis and design of the control system. Thus, the FLC is able to keep track the reference voltage in both transient and steady-state condition, stabilizing the inverter output voltage and frequency. Once synchronization with the grid is achieved, the controllable breaker connects the system to the grid. This is the current-controlled scheme, where the current is controlled and injected to the grid. The FLC tracks the desired current based on the error generated between the actual current components, I_d and I_q, and their respective reference currents, i.e., $I_{\rm dref}$ and $I_{\rm qref}$, which are generated previously in the voltage-controlled scheme. In this scheme, $V_{\rm dc}$ is compared with the reference voltage, i.e., $V_{\rm dcref}$, and an error is produced. This error is fed to the FLC for the error minimization. The output signal of the controller serves as a reference current, $I_{\rm dref}$ for the previously described current-controlled scheme.

The other part of the control system is the system protection algorithm. The operability is tested with the application the grid disturbances to the system, e.g., overvoltage, undervoltage, overfrequency, and underfrequency. Considering safety as the priority, the breaker contactor opens-up and the inverter shuts down in the present of abnormalities. e.g., grid voltage increase and decrease above 110% and below 88%, respectively, frequency increase and decrease above 51 Hz and below 49 Hz, respectively.

III. Proposed Fuzzy Logic Control

The basic architecture of the FLC used in the control strategy is shown in Fig. 3. The main elements that makes up a FLC system are the *fuzzifier* unit at the input terminal, knowledge

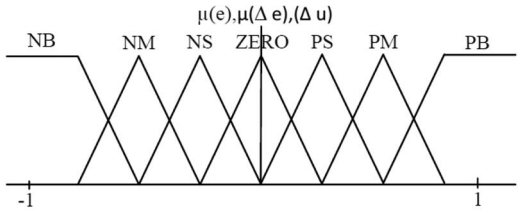

Δerror \ error	NB	NM	NS	ZE	PS	PM	PB
NB	NB	NB	NM	NM	NS	NS	ZE
NM	NB	NM	NM	NS	NS	ZE	PS
NS	NM	NM	NS	NS	ZE	PS	PS
ZE	NM	NS	NS	ZE	PS	PS	PM
PS	NS	NS	ZE	PS	PS	PM	PM
PM	NS	ZE	PS	PS	PM	PM	PB
PB	ZE	PS	PS	PM	PM	PB	PB

Fig. 4. Membership functions for error, change of error, controller output, and rule-based matrix table.

based (rule base) and the inference engine, and *defuzzifier* at the output terminal. In FLC-based control system, the required variables are the input and output variables. The inputs to the FLC are the parameters or variables of the process to be controlled, which depend on the applications. Normally, an error and its rate of change are chosen for the input variables. Meanwhile, the change of current and voltage are selected to be the output variables. An error in discrete time is the difference between the desired output or reference, $r(k)$, and the process output variable, $y(k)$. The current sample of error, $e(k)$ and the change of error $\Delta e(k)$ are defined in (6) and (7), respectively.

These variables universal discourse, which are normalized to fit into the interval value between -1 and $+1$, require seven membership functions, as shown in Fig. 4. Any input, which is not in this range, is considered too big and generate large error signals. For simplification, the triangular and trapezoidal membership functions are utilized. Using triangular and trapezoidal membership functions, the controller manages to reduce the error signal in a faster manner that increases the system transient response. The membership functions are labeled as NB for "Negative Big," NM for "Negative Medium," NS for "Negative Small," ZE for "Zero," PS for "Positive Small," PM for "Positive Medium" and PB for "Positive Big." The input variables are fuzzified through these membership functions

$$e(k) = r(k) - y(k) \tag{6}$$

$$\Delta e(k) = e(k) - e(k-1). \tag{7}$$

By the essence of the inference process and with the aid of the knowledge-based rules, the fuzzy output is generated. The important part of the FLC is the knowledge-based element, which consists of a list of fuzzy rules [32]. The inference process is to generate a fuzzy output set according to the IF-THEN rules. With these rules, the fuzzy controller behaves intelligently and capable of imitating humanlike-decision. There are 49 rules of "IF-THEN" logic related to the inputs and outputs, as shown in Fig. 4. This logic makes the control function into an FLC. From the figure, some of the rules are as follows:

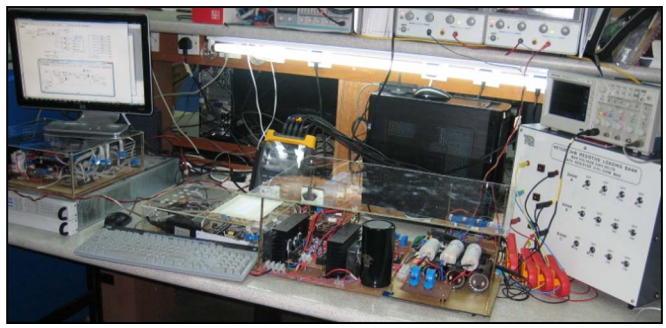

Fig. 5. Test setup for prototype PV-based grid-connected inverter system.

Rule 1: IF "error (e)" is NB AND "Δerror(Δe)" is NB THEN Δu is NB
Rule 2: IF "error" is NM AND "Δerror" is NB THEN Δu is NB
Rule 3: IF "error" is NS AND "Δerror" is NB THEN Δu is NM
Rule 4: IF "error" is ZE AND "Δerror" is NB THEN Δu is NM
Rule 5: IF "error" is PS AND "Δerror" is NB THEN Δu is NS
- -
Rule 49: IF "error" is PB AND "Δerror" is PB THEN Δu is PB

In the system implementation, the fuzzy controller output, $u(k+1)T_s$, keep changing in every sampling time until it reaches a steady-state condition, as described in (8) [33]

$$u(k+1) = u(k) + \Delta u(k) \tag{8}$$

where $\Delta u(k)$ is the sample of controller output. In this paper, the center of area *defuzzification* method is used to calculate the actual output from its fuzzy value as given in (9). It is a simple and accurate technique, which finds the "balance" point of the solution region by calculating the weighted mean of the fuzzy region

$$u = \frac{\sum_{i=1}^{k} u_i \times \mu(u_i)}{\sum_{i=1}^{k} \mu(\mu_i)} \tag{9}$$

where $\mu(u_i)$ is membership value of the combined membership function corresponding to each rule.

IV. DSP-Based Prototype Implementation

In order to validate the effectiveness of the proposed algorithms in real time, the proposed FLC-based PV grid-connected inverter system is experimentally implemented using dSPACE DSP board DS1104 [34]. The control algorithm is specifically designed for the PV application whereby its output power fluctuates depending on the solar irradiation levels. The experimental test set up for the 3 kW prototype PV-based grid-connected three-phase inverter is shown in Fig. 5. The dc power source is provided by the 3 kW solar panels of Solartif STF-120P6PV, as shown in Fig. 6. The solar panel requires open-circuit voltage

Fig. 6. Solar panels used in the experiment.

TABLE II
DEVELOPED INVERTER PROTOTYPE'S PARAMETERS

Parameter	Meaning	Value/model
V_{dc}	Dc link voltage	700V
$S_1 - S_7$	Switching signals for IGBTs	IXDR30N120D1
C_{dc}	Dc link capacitor	$4300\mu F$
F_{tri}	IGBT switching frequency	15 kHz
L_{filter}	Filter inductance	1.8 mH
C_{filter}	Filter capacitance	30 μF
Topology	Three-phase	-
Switching Technology	SPWM	-

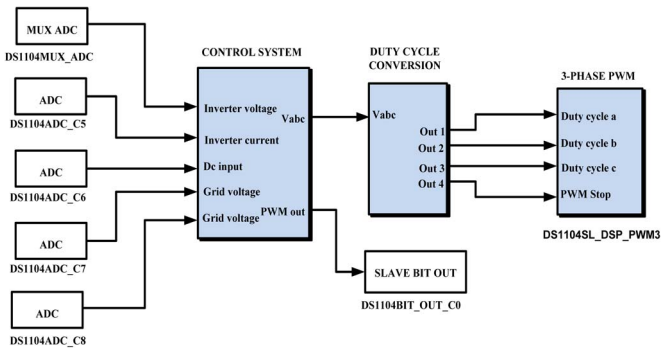

Fig. 7. Real-time Simulink model of three-phase inverter.

of 21.5 V, short-circuit current of 7.63 A, maximum power at voltage 17.40 V and current 6.89 A. The inverter accepts dc input voltage of 700 V from the boost converter and generates output voltage of 240 V at frequency of 50 Hz. With filter parameter of 1.8 mH, the output waveforms require low THD. The DSP board DS1104 is installed inside a personal computer with uninterrupted communication capability through a dual port memory. The DS1104 board is mainly based on a 64-bit PowerPC type PPC603e processor. The DSP is supplemented by a set of on-board peripherals used in digital control systems, including analog to digital (A/D), digital to analog (D/A) converters and digital incremental encoder interfaces. The detail parameters of the developed prototype are shown in Table II.

For real-time implementation, the real-time Simulink model, as shown in Fig. 7 is developed and then downloaded to the DSP board using the MATLAB/Simulink real-time workshop (RTW) tool and dSPACE ControlDesk software. With the application of the dSPACE graphical user interface (GUI) software, the monitoring of the performance and behavior of the inverter in real time is made possible. Moreover, the user is able to alter the controller parameters and immediately observe the effect of the system performance in real time as well.

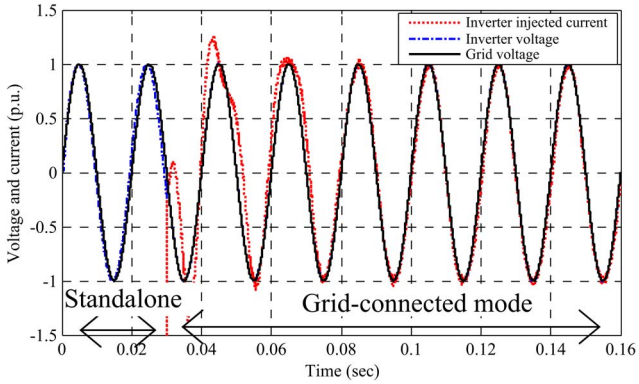

Fig. 8. Inverter injected current, inverter voltage, and grid voltage.

V. RESULTS AND DISCUSSION

The prototype grid-connected PV inverter control system was tested at different scenarios such as load variation, grid voltage and frequency disturbances. Sample results are presented in the following. During normal synchronization of the inverter with grid, Fig. 8 shows the tested waveforms of inverter output voltage, injected current and grid voltage for one phase for a period of 0.16 s with a sampling period of 5 μs.

It is seen from this figure that all the waveforms are nearly sinusoidal with a frequency of 50 Hz and having peak voltages of 1.0 p.u. This is equivalent to rms phase voltage of 240 V or line voltage of 415 V. Initially, the system is started in a standalone mode operating as a voltage-controlled inverter. Then, the inverter requires the grid frequency and phase, thus make it possible to connect to the grid. Once synchronized, the grid-connecting switch is closed and the system operated in a grid-connected mode and behaved as a current-controlled inverter at 0.03 s. This is an important feature that a PV grid-connected inverter should require in order to connect to the grid safely. It can be seen that the voltage is kept constant during the period of connection with the grid, as to provide constant power flow to the grid. The injected current achieved in-phase condition with the grid voltage (unity power factor) except at the beginning of the connection due to some control algorithm delay. During the grid-connected mode, the system operated in current-control scheme and the behavior of the reference-current tracking can be seen with very small ripples in the current waveform. The role of the FLC in regulating the injected current to the grid was depicted by the constant level of the current waveform. In other words, the inverter was able to transfer the constant PV power to the grid and load.

It is important to know the power flow of the PV grid-connected inverter system. The inverter system power flow is shown in Fig. 9. For the period of 0 to 0.05 s, the load demand is 5.8 kW, which is considered as 100% load scenario, there is almost no power flowing to the grid. This is due to a power

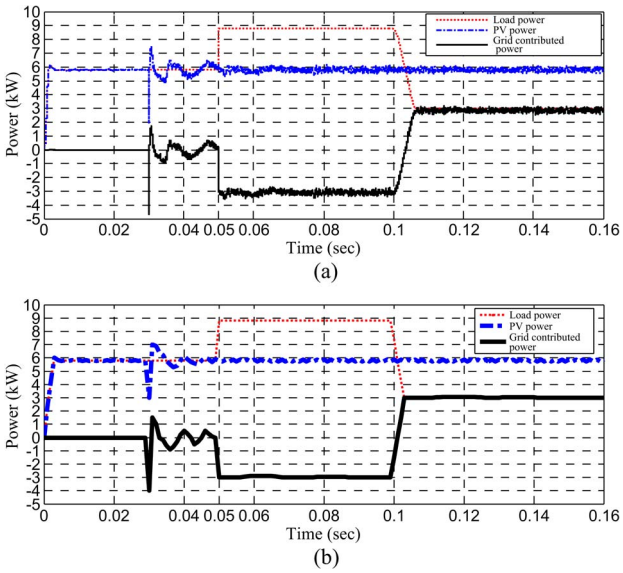

Fig. 9. Inverter system power flow using (a) PI controller and (b) FLC controller.

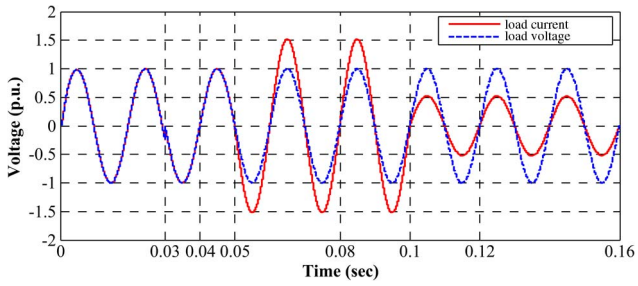

Fig. 10. Load voltage and current waveforms during load demand variation.

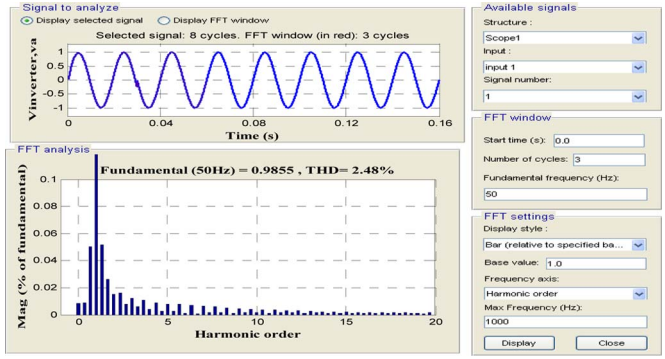

Fig. 11. THD and harmonics spectrum of inverter output voltage.

balance condition between PV and load, where the generated power is equal to the power demand. During the grid-connected mode, from 0.05 to 0.1 s, the load power is increased to 8.8 kW. This is considered as 150% load scenario, which is equivalent to an increase of 3 kW. This is a condition where the load demands more power from the PV. Since PV has the capacity of 5.8 kW, the additional balance of power is drawn from the grid, which is indicated by -3 kW in the grid contribution profile in the figure. The grid continues to supply power to the load until 0.1 s., when the load is reduced to 3.0 kW. This is a 50% load scenario, where the load uses less power compared with the generated one. Hence, the excess power from the PV, which is approximately 3 kW is dispatched to the grid, which shown by the $+3.0$ kW in grid contribution profile line. The analysis of power flow scenarios has demonstrated the ability of the inverter to extract power from the PV and feed to the load and grid.

A small step transient condition is observed when switching the inverter from stand-alone mode to grid-connected mode, as shown in Fig. 9. However, the developed FLC controller compensates the overall transient effects and the system come down to steady-state condition quickly. The short transient condition happens due to the tedious FLC tuning and curse of dimensionality to set up the rules.

In general, a grid-connected system is in invariantly rich transient conditions. PV-based grid-connected system accommodates both the power versatility of solar radiations and the frequency and system load variations. It is seen that using PI controller, inverter system exhibit much transients and overshoots effect in PV and grid-contributed power compare to FLC controller, as shown in Fig. 9(a). However, the developed FLC controller compensates the overall transient effects and the system come down to steady-state condition quickly, as shown in Fig. 9(b). The short transient condition happens due to the tedious FLC tuning and curse of dimensionality to set up the rules.

The corresponding load voltage and current waveforms during the load demand variations are shown in Fig. 10. Both waveforms are in phase during the load variations period. An increased of the load power demand beyond the PV capacity has caused the additional power drawn from the grid. This is shown by the current waveform during the period of 0.05 to 0.1 s. A drop of load power demand after 0.1 s onward has shown a decreasing of load current. Consequently, the excess of PV power was exported to the grid. Importantly, the load voltage was kept constant regardless of the load power profile as to provide constant power flow to the load and grid.

The criterion of having quality output power acquiring lower voltage and current harmonic contents for the inverter is important particularly when connecting to the grid. By utilizing the fast Fourier transform (FFT) technique, the THD of the phase voltage and current waveforms are calculated to be 2.48% and 4.64%, respectively. These levels are below 5% and hence, complied with the IEEE Std. 929-2000 [30]. The waveforms and their respective harmonics spectrums are shown in Figs. 11 and 12. The harmonic levels are resulted from the effectiveness of the control algorithm that employs the FLC, sinusoidal PWM (SPWM) technique, voltage, and current-controlled algorithms, and filter.

The performance of the FLC and PI controller are evaluated in terms of transient and steady-state response in stabilizing the dc-link voltage for ensuring low ripple on the inverter ac output waveform. During the stand-alone mode, FLC exhibited good response with no overshoot during the initial stage of the transient response, as shown in Fig. 13. Unlike the FLC, PI controller transient response shows an overshoot occurred at the starting point before stabilized, which is shown in Fig. 14. The steady-state response characteristic for the grid-connected mode was considered good for both controllers as can be seen after $t = 0.04$ s onward.

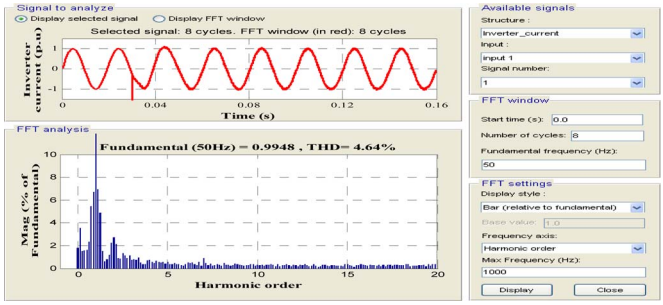

Fig. 12. THD and harmonics spectrum of inverter output current.

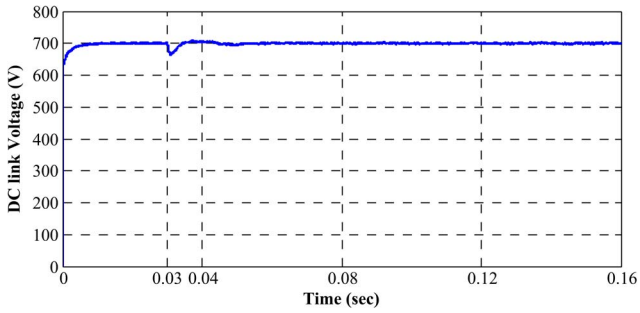

Fig. 13. DC-link voltage waveform controlled by FLC.

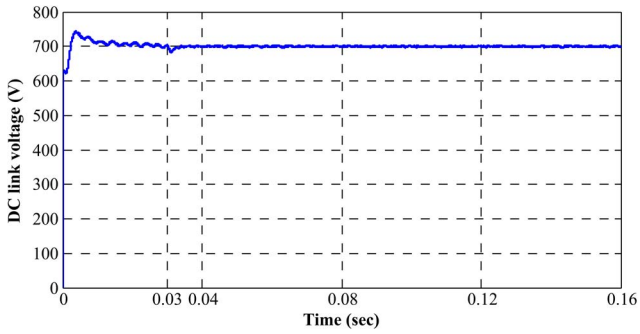

Fig. 14. DC-link voltage waveform controlled by PI.

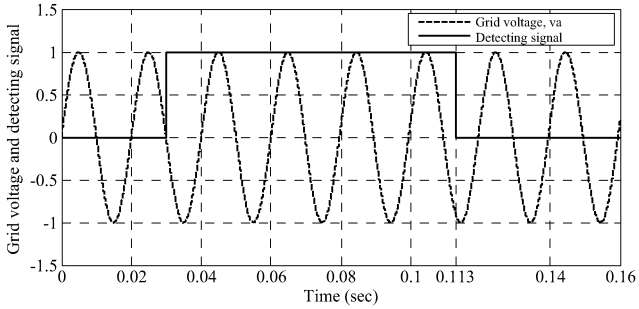

Fig. 15. Grid voltage and detecting signal during frequency increase.

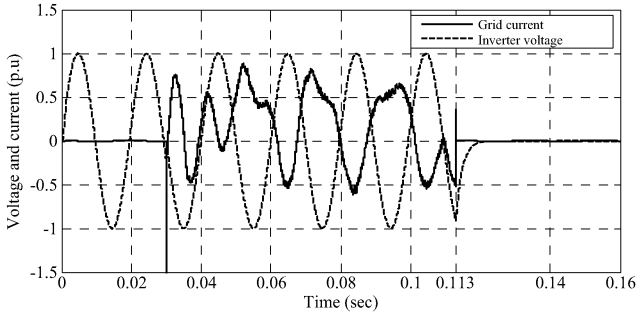

Fig. 16. Grid current and inverter voltage for grid frequency increase.

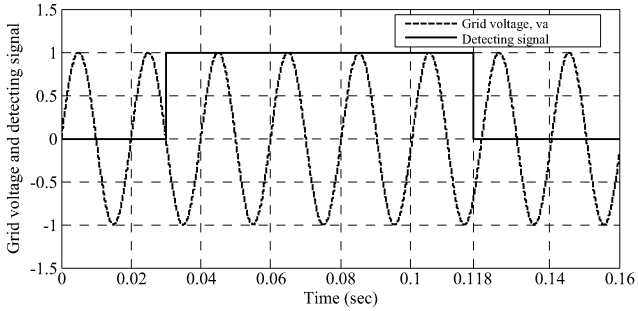

Fig. 17. Grid voltage and detecting signal during frequency decrease.

The inverter behaviors during grid disturbances such as overvoltage, undervoltage, overfrequency, and underfrequency are shown in the following figures. Such disturbances are purposely applied in order to access to ability of the inverter control algorithm to handle disturbances in a safely and properly manner. Such responses were evaluated based on [35], which stated that the inverter should cease to energize the utility line in the conditions, where the grid voltage increased above 110% (264 V) and dropped below 88% (211 V) of the nominal voltage, i.e., 240 V. As for the frequency, the inverter system was evaluated for the frequency increased above 51 Hz and decreased below 49 Hz. The disturbances were introduced for a time period of 0.06 to 0.095 s.

Figs. 15 and 16 show the overfrequency situation when the grid frequency was increased to 51 Hz. Initially, the inverter was in a stand-alone mode that is shown by the zero grid current. Then, at 0.03 s, it is connected to the grid. After detecting the disturbance, which occurred from 0.06 to 0.09 s, the inverter disconnected itself from the grid, and then shut down at 0.113 s. The isolation process, which is the moment of the disturbance occurrence to the time of grid disconnection, was approximately 2.65 cycles. It complies with the requirement of IEEE Std. 929-2000. This is shown in Fig. 16, where at 0.113 s onward, the inverter voltage and grid supplied current were zero, resulted from the inverter shutting down based on grid-isolating algorithm to provide safety protections.

The underfrequency scenario when the grid frequency dropped to 49 Hz is shown in Figs. 17 and 18. The inverter started with the stand-alone mode, operating with zero grid current, and then connected to the grid at 0.03 s. The inverter has detected the disturbance which occurred at 0.065 s, and then turned off and isolated itself from the grid at 0.118 s. Like the overfrequency case, the inverter shutting down and isolating process took about 2.65 cycles, which is within the range of the IEEE Std. 929-2000. As important as in the overfrequency scenario, the underfrequency disturbance occurrence should be managed so that device and personnel protection are guaranteed. This is shown from Fig. 18 where at 0.118 s onward, the inverter voltage and grid supplied current were zero, owing to the inverter shutting down based on grid-isolating algorithm.

Figs. 19 and 20 show the inverter reaction when detecting grid voltage increase to 264 V. Initially, the inverter operated in

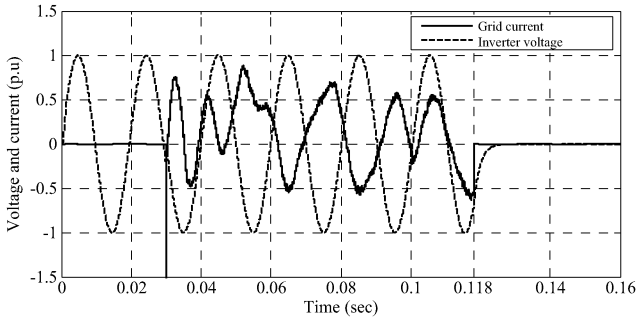

Fig. 18. Grid current and inverter voltage for grid frequency decrease.

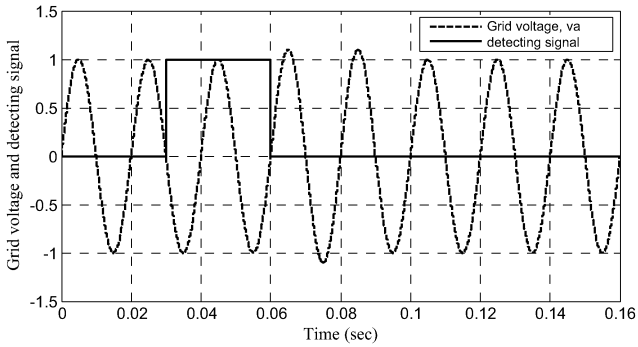

Fig. 19. Detecting signal for grid voltage increase.

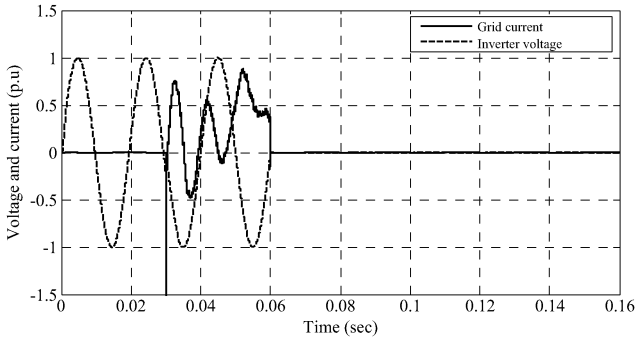

Fig. 20. Grid current and inverter voltage during grid voltage increase.

stand-alone mode and then started to connect to the grid at 0.03 s. This is shown by the "high" voltage level of the detecting signal. The inverter has detected the grid overvoltage disturbance which occurred at 0.0625 s and then caused the detecting signal to become "low" level, disconnecting it from the grid and switched off the inverter simultaneously. Consequently, there was no grid current flowing through and the inverter terminal voltage became zero, which is shown in Fig. 20.

The inverter behavior when the grid voltage dropped to 211 $V_{\rm rms}$ is shown in Figs. 21 and 22. Initially, the inverter was in stand-alone mode and then started to connect to the grid at 0.03 s. This is shown by the "high" voltage level of the detecting signal. The grid undervoltage disturbance was set at 0.065 s. Upon detection, the control system has caused the detecting signal to become "low" level, isolating it from the grid and immediately switched off the inverter. As a result, no grid current flowing through and the inverter terminal voltage became zero, as shown in Fig. 22.

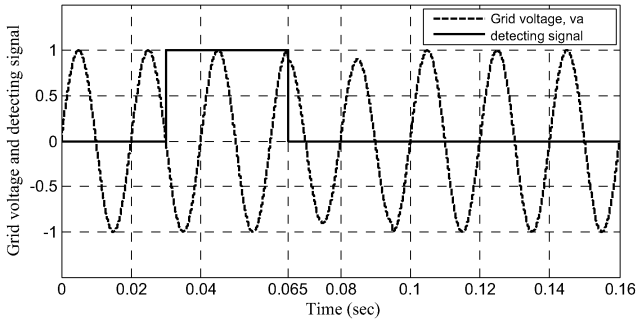

Fig. 21. Inverter voltage and grid current for grid voltage decrease.

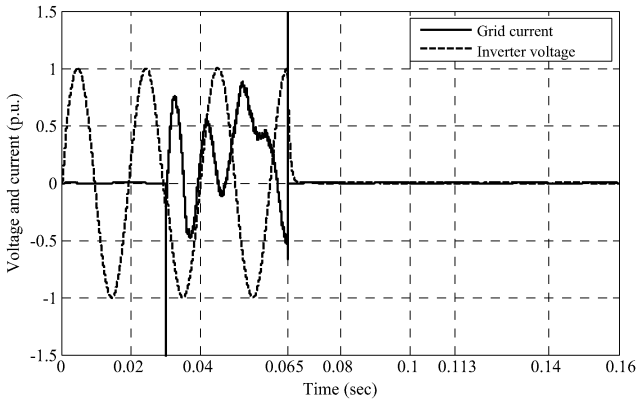

Fig. 22. Grid current and inverter voltage during grid voltage decrease.

The transient behavior of grid current during the period of grid connection with the inverter shows decaying and distorted features under increased and decreased frequencies and voltage conditions. This happened due to increased load power demand, which, in turn, exhibits 180° out of phase between grid current and inverter voltage. In general, grid requires sinusoidal ac with stable voltage and frequency; however, this test is conducted at increased and decreased frequencies and voltage conditions to observe the controller efficiency. It is observed that upon detecting the deviation from the nominal condition, the control algorithm isolates the PV-based inverter system from the grid and immediately switched off the inverter.

VI. Conclusion

The modeling and real-testing of a specific FLC for high-performance control of a grid-connected three-phase PV inverter have been presented in this paper. The control algorithm was implemented in real time using DSP controller board DS1104. The prototype system has been tested for different loads, the grid voltage and frequency disturbance scenarios. The obtained results showed that the inverter control system employing FLC is very effective in producing stable and nearly sinusoidal waveforms of both voltage and current. Moreover, the inverter is able to transfer the available excess PV power to the utility grid. In addition, the inverter has successfully detected the occurrences of grid disturbances and capable of disconnecting it from the grid as to provide protection for both device and personnel. Real-time results showed that the

proposed fuzzy logic controlled PV inverter system is capable of generating quality PV power to the grid, maintaining unity power factor and handling the grid voltage/frequency disturbances. Thus, the developed control system is found very effective and practical for the prototype realization of PV-based grid-connected system utilizing DS1104 controller board.

REFERENCES

[1] A. Zahedi, "A review of drivers, benefits, and challenges in integrating renewable energy sources into electricity grid," *Renew. Sustain. Energy Rev.*, vol. 15, no. 9, pp. 4775–4779, Dec. 2011.

[2] G. Kyriakarakos, A. I. Dounis, K. G. Arvanitis, and G. Papadakis, "A fuzzy logic energy management system for polygeneration microgrids," *Renew. Energy*, vol. 41, pp. 315–327, May 2012.

[3] H. Jiayi, J. Chuanwen, and X. Rong, "A review on distributed energy resources and microgrid," *Renew. Sustain. Energy Rev.*, vol. 12, no. 9, pp. 2472–2483, Dec. 2008.

[4] J. D. Mondol, Y. G. Yohanis, and B. Norton, "The impact of array inclination and orientation on the performance of a grid-connected photovoltaic system," *Renew. Energy*, vol. 32, no. 1, pp. 118–140, Jan. 2007.

[5] M. Datta, T. Senjyu, A. Yona, and T. Funabashi, "A fuzzy based method for leveling output power fluctuations of photovoltaic-diesel hybrid power system," *Renew. Energy*, vol. 36, no. 6, pp. 1693–1703, Jun. 2011.

[6] F. Botteron and H. Piheiro, "Descrete-time internal model controller for three-phase PWM inverters with isolator transformer," *Proc. Inst. Elect. Eng.—Elect. Power Appl.*, vol. 153, no. 1, pp. 57–67, Jan. 2006.

[7] M. A. Hannan, Z. A. Ghani, and A. Mohamed, "An enhanced inverter controller for PV applications using the dSPACE platform," *Int. J. Photoenergy*, vol. 2010, 2010, Art. ID. 457 562.

[8] L. Hassaine, E. Olias, J. Quintero, and M. Haddadi, "Digital power factor control and reactive power regulation for grid-connected photovoltaic inverter," *Renew. Energy*, vol. 34, no. 1, pp. 315–321, Jan. 2009.

[9] M. Sreedevi and P. J. Paul, "Fuzzy PI controller based grid-connected PV system," *Int. J. Soft Comput.*, vol. 6, pp. 11–15, 2011.

[10] A. Hmidet, R. Dhifaoui, and O. Hasnaoui, "Development, implementation and experimentation on a dSPACE DS1104 of a direct voltage control scheme," *J. Power Electron.*, vol. 10, no. 5, pp. 468–476, Sep. 2010.

[11] S. Alepuz *et al.*, "Interfacing renewable energy sources to the utility grid using a three-level inverter," *IEEE Trans. Ind. Electron.*, vol. 53, no. 5, pp. 1504–1511, Oct. 2006.

[12] N. A. Rahim, J. Selvaraj, and C. Krismadinata, "Five-level inverter with dual reference modulation technique for grid-connected PV system," *Renew. Energy*, vol. 35, no. 3, pp. 712–720, Mar. 2010.

[13] P. Bhubaneswari, S. Iniyan, and G. Ranko, "A review of solar photovoltaic technologies," *Renew. Sustain. Energy Rev.*, vol. 15, no. 3, pp. 1625–1636, Apr. 2011.

[14] E. K. Ahmad, N. A. Rahim, and J. Selvaraj, "Optimized PID controller for both single phase inverter and MPPT SEPIC DC/DC converter of PV module," in *Proc. IEEE Int. Elect. Mach. Drives Conf.*, 2011, pp. 1036–41.

[15] A. Kulkarni and V. John, "Mitigation of lower order harmonics in a grid-connected single-phase PV inverter," *IEEE Trans. Power Electron.*, vol. 28, no. 11, pp. 5024–5037, Nov. 2013.

[16] A. Luo, Y. Chen, Z. Shuai, and C. Tu, "An improved reactive current detection and power control method for single-phase photovoltaic grid-connected DG system," *IEEE Trans. Energy Convers.*, vol. 28, no. 4, pp. 823–831, Dec. 2013.

[17] S. Mishra, D. Ramasubramanian, and P. C. Sekhar, "A seamless control methodology for a grid connected and isolated PV-diesel microgrid," *IEEE Trans. Power Syst.*, vol. 28, no. 4, pp. 4393–4404, Nov. 2013.

[18] Q. Hengsi and J. W. Kimball, "Closed-loop control of DC-DC dual active bridge converters driving single-phase inverters," *IEEE Trans. Power Electron.*, vol. 29, no. 2, pp. 1006–1017, Feb. 2014.

[19] C. Cecati, F. Ciancetta, and P. Siano, "A multilevel inverter for photovoltaic for photovoltaic systems with fuzzy logic control," *IEEE Trans. Ind. Electron.*, vol. 57, no. 12, pp. 4115–4125, Dec. 2010.

[20] D. O. Abdeslam, P. Wira, J. Merckle, and D. Flieller, "Artificial neural networks to control an inverter in a harmonic distortion compensation scheme," in *Proc. IEEE Int. Symp. Ind. Electron.*, 2008, pp. 1879–1884.

[21] T. Govindaraj and N. M. Dhivya, "Simulation modelling on artificial neural network based voltage source inverter fed PMSM," *Int. J. Innov. Res. Elect., Electron., Instrum. Control Eng.*, vol. 2, no. 1, pp. 785–792, Jan. 2014.

[22] N. Altin and I. Sefa, "Simulation of neuro-fuzzy controlled grid-connected inverter," in *Proc. XXIII Int. Symp. Commun. Autom. Technol.*, Oct. 27–29, 2011, pp. 1–7.

[23] E. Koutroulis and F. Blaabjerg, "Methods for the optimal design of grid-connected PV inverters," *Int. J. Renew. Energy Res.*, vol. 1, no. 2, pp. 54–64, 2011.

[24] P. Garcia, C. A. Garcia, L. M. Fernandez, F. Llorens, and F. Jurado, "ANFIS-based control of a grid-connected hybrid system integrating renewable energies, hydrogen and batteries," *IEEE Trans. Ind. Informat.*, vol. 10, no. 2, pp. 1107–1117, May 2014.

[25] S. Premrudeepreechacharn and T. Poapornsawan, "Fuzzy logic control of predictive current control for grid-connected single phase inverter," in *Proc. 28th IEEE Photovoltaic Spec. Conf.*, 2000, pp. 1715–1718.

[26] L. Pisit, P. Serge, and M. T. Farid, "Nonlinear control techniques of a controllable rectifier/inverter-motor drive system with a small DC-link capacitor," *Energy Convers. Manage.*, vol. 49, no. 12, pp. 3541–3549, Dec. 2008.

[27] C. L. Poh and G. H. Donald, "Analysis of multiloop control strategies for LC/CL/LCL-filtered voltage-source and current-source inverters," *IEEE Trans. Ind. Appl.*, vol. 41, no. 2, pp. 644–654, Mar./Apr. 2005.

[28] L. Shuhui, T. A. Haskew, L. Dawen, and H. Fei, "Integrating photovoltaic and power converter characteristics for energy extraction study of solar PV systems," *Renew. Energy*, vol. 36, no. 12, pp. 3238–3245, Dec. 2011.

[29] Subiyanto, A. Mohamed, and M. A. Hannan, "Intelligent maximum power point tracking for PV system using hopfield neural network optimized fuzzy logic controller," *Energy Buildings*, vol. 51, pp. 29–38, Aug. 2012.

[30] P. J. Perez, G. Almonacid, J. Aguilera, and J. Casa, "RMS current of a photovoltaic generator in grid-connected PV systems: Definition and application," *Int. J. Photoenergy*, vol. 2008, 2008, Art. ID. 356 261.

[31] K. Bandara, T. Sweet, and J. Ekanayake, "Photovoltaic applications for off-grid electrification using novel multi-level inverter technology with energy storage," *Renew. Energy*, vol. 37, no. 1, pp. 82–88, Jan. 2012.

[32] D. K. Chaturvedi, *Modeling and Simulation of Systems Using MATLAB and Simulink*. Boca Raton, FL, USA: CRC Press, 2006.

[33] Z. Kovacic, and S. Bogdan, *Fuzzy Controller Design: Theory and Applications*. Boca Raton, FL, USA: CRC Press, 2006.

[34] dSPACE DS1104, Hardware Installation and Configuration and ControlDesk Experiment Guide, dSPACE, Paderborn, Germany, 2008.

[35] *Recommended Practices for Utility Interface of Photovoltaic System*, IEEE Std 929-2000, 2002.

M. A. Hannan received the B.Sc. degree in electrical and electronic engineering from the Chittagong University of Engineering and Technology, Chittagong, Bangladesh, in 1990, and the M.Sc. and Ph.D. degrees in electrical, electronic, and systems engineering from the Universiti Kebangsaan Malaysia (UKM), Bangi, Malaysia, in 2003 and 2007, respectively.

Currently, he is a Professor with the Department of Electrical, Electronics, and Systems Engineering, UKM. His research interests are in intelligent signal processing, intelligent embedded systems, intelligent inverter controllers, and artificial intelligence.

Zamre Abd. Ghani received the B.Sc. degree in electrical engineering from the University of the Pacific, Stockton, CA, USA, the M.Eng. degree in electrical engineering from the Universiti Teknologi Malaysia (UTM), Johor, Malaysia, and the Ph.D. degree in electrical, electronic and systems engineering from the Universiti Kebangsaan Malaysia (UKM), Bangi, Malaysia, in 1987, 2007, and 2014, respectively.

Currently, he is a Senior Lecturer with the Department of Industrial Electronics, Faculty of Electronic and Computer Engineering, Universiti Teknikal Malaysia (UTeM) Melaka, Melaka, Malaysia. His main research interests are power electronic controllers for photovoltaic applications such as inverters and dc–dc converters.

Azah Mohamed (M'90–SM'03) received the B.Sc. degree from the University of London, London, U.K., in 1978 and the M.Sc. and Ph.D. degrees from the Universiti Malaya, Kuala Lumpur, Malaysia, in 1988 and 1995, respectively.

She is a Professor with the Department of Electrical, Electronic and Systems Engineering, Universiti Kebangsaan Malaysia, Bangi, Malaysia. Her main research interests are in power system security, power quality, and artificial intelligence.

M. Nasir Uddin (S'99–M'00–SM'04) received the B.Sc. and M.Sc. degrees in electrical and electronic engineering from Bangladesh University of Engineering and Technology (BUET), Dhaka, Bangladesh, and the Ph.D. degree in electrical engineering from Memorial University of Newfoundland (MUN), St. John's, NF, Canada, in 1993, 1996, and 2000, respectively.

Currently, he is a Professor with the Department of Electrical Engineering, Lakehead University, Thunder Bay, ON, Canada, where he is engaged in teaching and research. His research interests include power electronics, electric motor drives, and applications of neural networks.